RSC Advances

GaN:Pr^{3+} nanostructures for red solid state light emission

Journal:	*RSC Advances*
Manuscript ID:	RA-ART-08-2014-008571.R2
Article Type:	Paper
Date Submitted by the Author:	12-Nov-2014

Complete List of Authors:	Rodrigues, Joana; Universidade de Aveiro, Department of Physics & i3N Ben Sedrine, Nabiha; Universidade de Aveiro, Departamento de Física & I3N Felizardo, Miguel; Instituto Superior Técnico, Universidade de Lisboa, Campus Tecnológico e Nuclear Soares, Jorge; University of Aveiro, Department of Physics Alves, Eduardo; Instituto Superior Técnico, Universidade de Lisboa, Campus Tecnológico e Nuclear Neves, Armando; Universidade de Aveiro, Departamento de Física & I3N Fellmann, Vincent; Univ. Grenoble Alpes, CEA/CNRS Group, "Nanophysique et Semiconducteurs" Tourbot, G.; Univ. Grenoble Alpes, CEA/CNRS Group, "Nanophysique et Semiconducteurs" Auzelle, Thomas; Univ. Grenoble Alpes, CEA/CNRS Group, "Nanophysique et Semiconducteurs" Daudin, B.; Univ. Grenoble Alpes, CEA/CNRS Group, "Nanophysique et Semiconducteurs" Bockowski, Michal; Institute of High Pressure Physics PAS, Pressurized Food and Soft Matter Lorenz, Katharina; Instituto Superior Técnico, Universidade Técnica de Lisboa, Monteiro, Teresa; Universidade de Aveiro, Departamento de Física & I3N

SCHOLARONE™
Manuscripts

RSC Advances RSCPublishing

ARTICLE

GaN:Pr^{3+} nanostructures for red solid state light emission

Cite this: DOI: 10.1039/x0xx00000x

Received 00th January 2012,
Accepted 00th January 2012

DOI: 10.1039/x0xx00000x

www.rsc.org/

J. Rodrigues[a*], N. Ben Sedrine[a], M. Felizardo[b], M. J. Soares[a], E. Alves[b,c], A. J. Neves[a], V. Fellmann[d], G. Tourbot[d], T. Auzelle[d], B. Daudin[d], M. Boćkowski[e], K. Lorenz[b,c], T. Monteiro[a]

Praseodymium implanted and annealed GaN films, quantum wells, nanowires and quantum dots were studied by photoluminescence. After implantation and annealing, Pr^{3+} intra-shell luminescence was achieved for all the analysed samples. In the trivalent charge state the ion luminescence was found to be dominated by the red lines of the $^3P_0 \rightarrow {}^3F_2$ transition. In the case of GaN films, an intense red emission is observed with naked eye at room temperature. Photoluminescence excitation indicates that the preferential population mechanisms of this emission are achieved by using excitation above the GaN band gap. A comparison of the optically active ion luminescence spectral shape and peak position in the different structures is established. For the GaN nanowires the $^3P_0 \rightarrow {}^3F_2$ lines of the Pr^{3+} ions are in good agreement with those identified in GaN films. In the case of GaN quantum dots the ion emission was found to be similar to that observed in AlN layers. For AlN/GaN/AlN quantum wells alike behaviour was identified with the sharp ion luminescence lines superimposed to a broad band likely generated by the overlap of multiple Pr-centres. The ion luminescence stability was analysed and discussed for all the studied samples.

Introduction

Gallium nitride (GaN) is a direct wide band gap material with gap energy E_g=3.4 eV [1] at room temperature (RT) which has been extensively studied for applications in optoelectronic devices. This material has been widely used as a host for the incorporation of luminescent activators such as rare-earth (RE) ions. As proposed by Favennec *et al.* [2] there is a direct correlation between the band gap of the host material and the optical efficiency of the RE^{3+} emission. The luminescence thermal quenching decreases with increasing band gap, which make wide band gap materials suitable for the RE^{3+} optical activation [3,4]. These ions give rise to luminescent transitions in a wide spectral region that can cover ultraviolet, visible and infrared [5–8]. Other advantages of the RE^{3+} ions include the sharp atomic-like emission lines associated with its $4f \rightarrow 4f$ intra-shell transitions and the fact that their spectral positions are almost insensitive to the host crystalline environment [3,9]. The trivalent praseodymium (Pr^{3+}) ion has a $4f^2$ configuration with $^3H_4$ ground state and $^3H_{5,6}$, $^3F_{2,3,4}$, $^1G_4$, $^1D_2$, $^3P_{0,1}$, $^1I_6$, $^3P_2$ and $^1S_0$ excited states [10]. This ion has been incorporated in nitride matrix in order to promote visible emission that arises from transitions between the crystal-field splitted energy levels of its $^{(2S+1)}L_J$ manifolds, especially in the red spectral region due to the intense emission of its $^3P_0 \rightarrow {}^3F_2$ transition [5,7,10–13]. Reported works of Pr^{3+} in different hosts revealed that the emission spectra of Pr^{3+} ions are very complex since they reveal ion-lattice interactions that broaden the pure electronic lines and contribute to a large number of vibronic lines [10,14,15].

The use of low dimensional GaN nanostructures such as quantum wells (QWs), nanowires (NWs) and quantum dots (QDs) has gained a very much interest in lighting devices. In the case of the NWs, their non-planar geometry is expected to lead to an increase in light-extraction efficiency [16,17]. Other advantages include the compatibility with highly mismatched substrates, the absence of extended defects and the efficient release of any strain by surface relaxation [16]. The use of GaN quantum structures like QWs or QDs also offers some benefits due to the spatial confinement effects of the carriers [18,19]. For instance, QDs can capture carriers that will occupy strongly localized states limiting their migration toward the defects that are formed during the growth process [18]. Previous reported works revealed that GaN QDs grown in a AlN matrix can be efficient light emitters even when grown on highly mismatched substrate such as silicon [18,20]. RE-doped GaN and AlN layers usually present considerable nonradiative carrier recombination channels which affect the intra-4*f* ion luminescence efficiency. Such processes are expected to be supressed with the incorporation of the RE^{3+} ions inside the quantum structures, by reducing the nonradiative decay paths due to the high crystal quality of GaN quantum structures [19,21].
In this work different GaN structures (films, QWs, NWs and QDs) were doped with Pr^{3+} ions by ion implantation. Post-implantation thermal annealing was performed in order to recover the lattice damage and promote the optical ion activation. The spectroscopic features of the doped structures were assessed by photoluminescence (PL). PL excitation (PLE) was recorded only for the films due to the low luminescence intensity of the nanostructures at room temperature (RT). All the implanted and annealed samples exhibit

This journal is © The Royal Society of Chemistry 2014

the intra-4f^{2} emission from the Pr^{3+}. The ion emission in the different GaN structures was analysed and the Pr^{3+} luminescence thermal quenching was compared and discussed.

Experimental details

GaN QD/AlN and GaN QW/AlN superlattice (SL) samples (20 periods SL) were grown by radio frequency plasma-assisted molecular beam epitaxy (MBE), as reported elsewhere [22,23]. GaN and AlN films grown by hydride vapour phase epitaxy (HVPE) on *c*-plane sapphire were purchased from TDI Oxford instruments (~3 •m). All these samples were implanted simultaneously with two different fluences: $1x10^{13}$ ions.cm^{-2} and $1x10^{15}$ ions.cm^{-2}, at the energy of 150 keV. In order to improve the optical activation, rapid thermal annealing (RTA) was performed during 30 s at 1200 ºC in flowing N_2 using an ANNEALSYS halogen lamp furnace. Only the GaN layers were annealed at 1400 °C during 30 minutes in high N_2-pressure (high temperature high pressure, HTHP); these are the optimised annealing conditions for implantation damage recovery and rare earth activation in GaN films [24,25]. The GaN NWs were grown by MBE on (111) Si substrates, as reported elsewhere [26]. A thin (2-3 nm) AlN buffer layer was deposited prior to the NWs growth which was performed for 2 hours at 880 ºC in nitrogen-rich conditions. The NWs samples were implanted with the same energy and fluences as the films. All implantations were carried out at RT and along the *c*-axis including the vertically aligned NWs. Post-implantation RTA of the NWs samples was performed for 30 s at 1000 ºC in flowing N_2 following best annealing conditions preserving the NWs [27]. A lower annealing temperature with respect to films, is necessary to suppress the dissociation of the GaN surface [28].

Scanning electron microscopy (SEM) measurements were acquired using a ZEISS Ultra 55 microscope.

Steady state PL was measured using the 325 nm light from a cw He-Cd laser and an excitation power density less than 0.6 W.cm^{-2}. The samples were mounted in a cold finger of a closed-cycle helium cryostat and the sample temperature was controlled in a range from 14 K to RT. The luminescence spectra were acquired using a dispersive system SPEX 1704 monochromator (1 m, 1200 grooves.mm^{-1}) fitted with a cooled Hamamatsu R928 photomultiplier tube.

For the infrared spectral region, the PL measurements were performed with a Bruker 66V Fourier transform spectrometer (FTIR).

The RT PLE was assessed in a Fluorolog-3 Horiba Scientific modular equipment with a double additive grating Gemini 180 scanning monochromator (2x180 mm, 1200 gr.mm^{-1}) in the excitation and a triple grating iHR550 spectrograph in the emission (550 mm, 1200gr.mm^{-1}). A 450 W Xe lamp was used as excitation source. The PLE was assessed by setting the emission monochromator in the maxima of the optically active defects and the excitation was scanned to higher energies. The measurements were realized using a front face acquisition mode, and were corrected to the optical components and to the Xe lamp spectral responses. RT lifetime measurements were acquired with the same Fluorolog-3 system using a pulsed Xe lamp and a DataStation software.

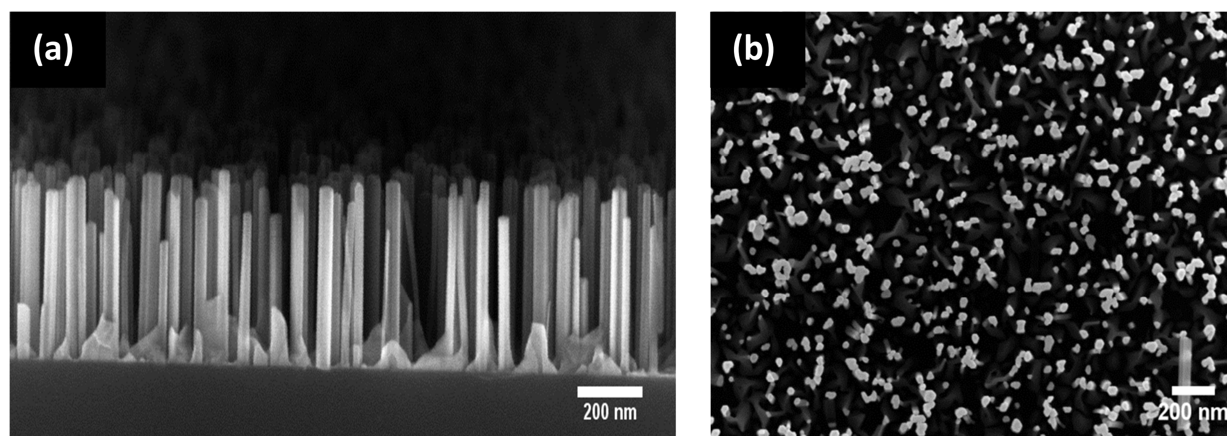

Figure 1 – (a) Side view and (b) plane view SEM images of the GaN nanowires before implantation.

Results and discussion

Figure 1 shows the SEM images of the NWs evidencing their good vertical alignment. The *c*-oriented NWs exhibit a length of ~ 300-400 nm with a diameter in the 20-50 nm range. Both GaN QD/AlN and GaN QW/AlN samples are composed by 20 periods of QDs or QWs with a height of ~ 2 nm, with an AlN spacer ~ 5 nm thick, as previously evidenced by SEM and TEM in earlier reported studies [29,30].

Figure 2 shows the 14 K PL spectra of the GaN films, NWs, QWs and QDs implanted with Pr^{3+} ions obtained under 325 nm photon excitation. After implantation and annealing all the analysed samples exhibit the emission lines associated with the intra-4f^{2} transitions of the Pr^{3+} ion, from which the most intense represents the red $^3P_0 \rightarrow ^3F_2$ multiplets transition. Besides the intraionic luminescence, other optically active centres are discriminated. Well resolved donor bound exciton (D^0X) and donor acceptor pair (DAP) transitions are clearly distinguished for GaN films and NWs implanted with low fluence. However for the QWs and QDs, the ultraviolet recombination broadens and the peak emission wavelength varies due to the balanced contributions of the spatial carrier confinement and the quantum confined stark effect (QCSE) [31]. As AlN layers are present in the QW and QDs structures, the observed ultraviolet recombination could arise from defects in the AlN films, such as oxygen-related and native defects as was previously reported [19,32,33]. In the case of the NWs implanted with higher fluence no near band edge (NBE) emission is observed, probably due to a higher implantation damage. Only a broad band observed in the violet region is identified in the spectral region of the DAP transitions, likely due to defects generated by implantation and annealing. In the

This journal is © The Royal Society of Chemistry 2014

longer wavelength region, a broad luminescence yellow band (YB) is observed in GaN films, QWs, NWs and QDs. Despite the similarities in the peak position and spectral shape of the YB, recent reports evidence a distinct recombination behaviour of the optical centres measured in GaN films and NWs. Particularly, the YB luminescence in films was associated to deep defect levels in GaN [34,35], while YB luminescence in NWs is mediated by surface states [17,36]. For the samples implanted with high fluence and regardless of the implantation damage recovery after thermal annealing treatments, a suppression of the band edge recombination in GaN films and QDs is observed.

Figure 3 depicts enlarged spectra of the intra-shell Pr^{3+} luminescence in the studied samples. As stated above, the most intense luminescence is due to the $^3P_0\rightarrow{}^3F_2$ transition that occurs in the red spectral region with the strongest RT Pr^{3+} luminescence observed in the GaN layer implanted with higher fluence. The peak positions and line assignments of the Pr^{3+} transitions identified in the studied samples are compiled in Table 1. The study will be focused on the transitions between the $^3P_0$ and $^3F_2$ multiplets shown in Figure 4. Unambiguous changes occur for the intraionic emission when the ion is incorporated in each studied structures. In the case of the GaN films, the most intense $^3P_0\rightarrow{}^3F_2$ lines obtained with above GaN bandgap excitation were found to occur at ~ 650.3 and 652.4 nm with a full with at half-maximum (FWHM) of ~0.2 nm, independently of the used ion fluence. These findings are in good agreement with previously reported data in praseodymium doped GaN layers [5,7,10]. The $^3P_0\rightarrow{}^3F_2$ lines in the GaN NWs were found to be similar to those of the GaN films although slightly displaced to short wavelengths. Since the peak position and the spectral shape of this luminescence agrees with those observed in the GaN films, the possibility that the ion emission originates from Pr^{3+} inside the AlN buffer layers can be disregarded, allowing to infer that the ions are effectively incorporated into the GaN NWs and occupy the Ga sites as reported for layers [13]. Additionally, the small wavelength shift in the peak position are likely due to different strain states of the GaN layers and NWs, since for the latter low strain levels are expected. Remarkable changes are noticed in the GaN QWs and GaN QDs embedded in AlN barriers. As a first remark we should emphasize that in both cases, and for the samples implanted with high fluence, shorter wavelength multiplet transitions from the Pr^{3+} ions were identified in the green spectral region (~526 nm) due to the $^3P_1\rightarrow{}^3H_5$ transition. This emission is usually very weak in GaN samples [10] and is more commonly observed in AlN layers and $Al_xGa_{1-x}N$ ternary alloys [5,7,37]. Such identification in the analysed QWs and QDs structures suggests that the optically active praseodymium ion in the mentioned samples is probably located inside AlN barriers or in regions where intermixing between QWs/QDs and barriers took place.

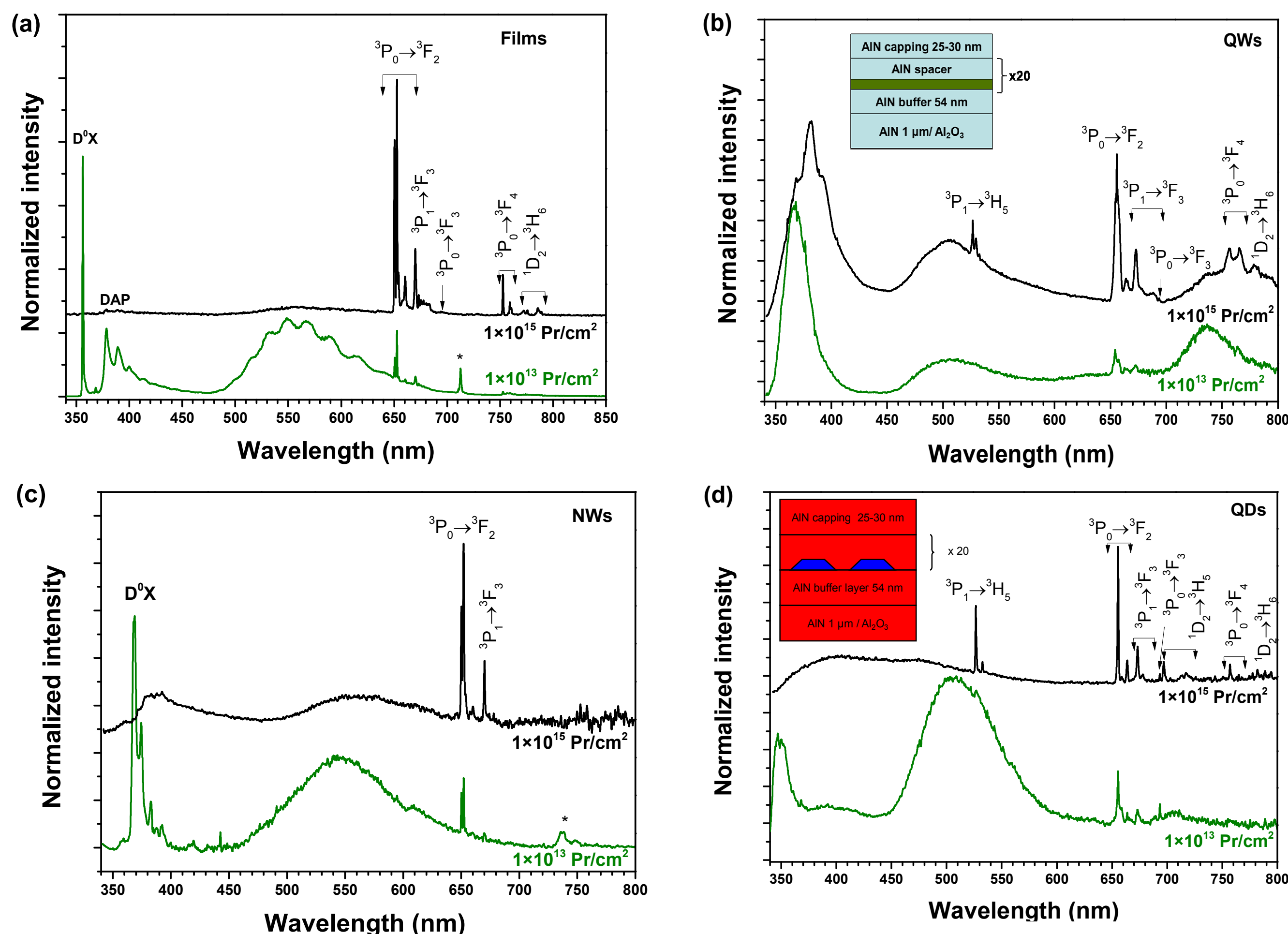

Figure 2 – Low temperature PL spectra of the GaN:Pr^{3+} (a) films, (b) QWs, (c) NWs and (d) QDs. The asterisk denotes the second order of the D^0X emission**.** All the spectra were acquired at 14 K with an excitation wavelength of 325 nm. The insets in (b) and (d) correspond to the QWs and QDs samples' structure, respectively.

Particularly, in the case of the QDs, the peak position and relative intensity of the $^3P_0 \rightarrow ^3F_2$ lines at ~654.6 nm and 655.6 nm are in fairly good agreement with those of Pr^{3+} observed in AlN layers [7]. Therefore, and independently of the used implantation fluence, the intraionic luminescence arises mainly from the Pr^{3+} inside the AlN spacers in the SL structure of GaN QDs embedded in the AlN spacers. This observation is in contrast to similar GaN QDs implanted with Eu, where the dominant Eu centre for low fluences was suggested to be Eu inside QDs [22], but it agrees well with the fact that the majority of the implanted Pr ions are expected to stop in the AlN barriers which account for ~90% of the implanted volume. An interesting behaviour is seen for the QW structure. Here, and for the sample implanted with the high fluence, Figure 4a evidences the $^3P_0 \rightarrow ^3F_2$ lines in the same position as those identified in the AlN layer in agreement with the fact that part of the optically active Pr^{3+} ions are located in the AlN host. Additionally the multiplet transitions are overlapped with a broad emission band similar to those bands previously reported for Pr^{3+} emission in $Al_xGa_{1-x}N$ layers with high aluminium content [5]. This may suggest a promotion of disorder-related effects after the implantation and annealing in the QW structure, generating intermixed AlGaN regions rich in aluminium. Argon implantation in the same GaN/AlN structures was recently shown to promote efficient intermixing in particular in GaN QD structures [23] while intermixing upon annealing is insignificant at the annealing temperatures used in this study [19,20,38]. However, for the case of the QW sample implanted with low fluence, where intermixing should be low, a similar overlap of emitting centres was found in the $^3P_0 \rightarrow ^3F_2$ spectral region. Also for the case of QDs the broad emission is seen only in the low fluence sample and much weaker than for the QW sample although it was shown that QDs reveal enhanced ion beam mixing [23]. Therefore it is unlikely that the broad emission lines are due to intermixed regions. Site multiplicity involving certain defects may be an alternative explanation. For the QW sample implanted with low fluence, a high energy shift of the $^3P_0 \rightarrow ^3F_2$ lines suggests that part of the praseodymium ions could be optically active in the GaN QWs. If there is the case, the shift of the dominant Pr^{3+} emission line to longer wavelengths (compared to the Pr^{3+} emission from GaN films) could be justified by different strain states of the GaN films and QWs. However, similar shifts to low energy of the peak position were found in $Al_xGa_{1-x}N$ layers with low x composition meaning that we cannot exclude that the ion luminescence arises from intermixed regions. In fact, this explanation likely elucidates the fact that no intraionic Pr^{3+} emission from the GaN layer was observed for the sample implanted with higher fluence.

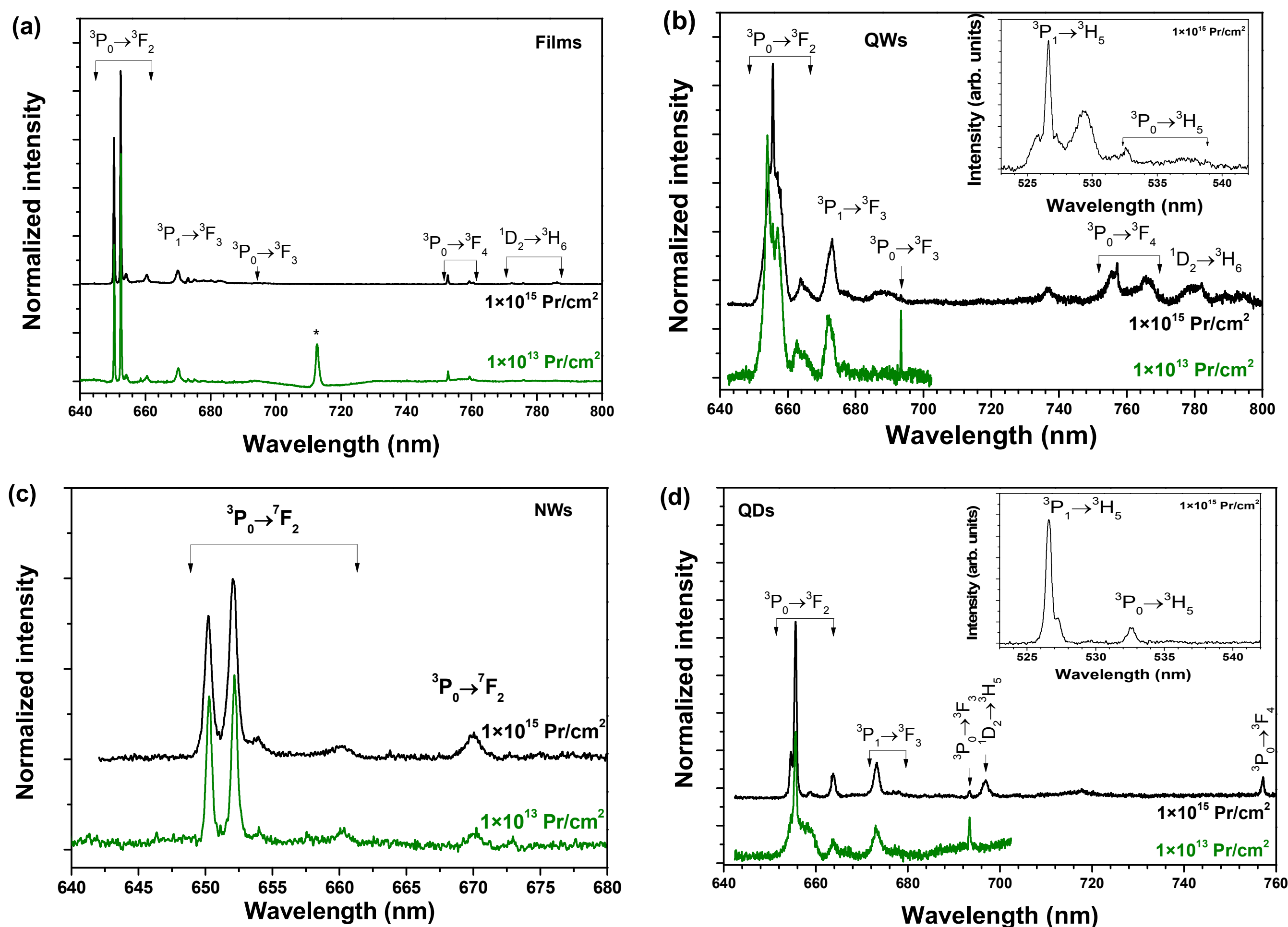

Figure 3 – High resolution low temperature PL spectra of the GaN:Pr^{3+} (a) films, (b) QWs, (c) NWs and (d) QDs recorded on the red-NIR region of the Pr^{3+} emission. The asterisk denotes the second order of the D^0X emission. The insets of figures (b) and (d) correspond to the ion

This journal is © The Royal Society of Chemistry 2014

emission on the green region of the electromagnetic spectrum. All the spectra were acquired at 14 K with an excitation wavelength of 325 nm.

Figure 5 depicts the temperature dependence of the $^3P_0 \rightarrow ^3F_2$ integrated intensity for the GaN films, NWs, QW and QD structures. For all studied samples it is shown that the intraionic luminescence decreases gradually with increasing temperature. The internal quantum efficiency of the ion luminescence, IQE, can be expressed as $IQE = \frac{W_{rad}}{W_{rad}+W_{nrad}}$, where $W_{rad} = \frac{1}{\tau_{rad}}$ stands for the radiative transition probability and $W_{nrad} = \frac{1}{\tau_{nrad}}$ is the nonradiative transition probability, which can be defined by a classical model. The nonradiative transition probability constitutes a thermally activated pathway for the depletion of the emitting state, which can be classically described by an activation energy, E_a. Following this approach the IQE value can be estimated by the ratio between the integrated ion emission at RT, $I_{PL}(RT)$, and low temperature, $I_{PL}(14\ K)$, assuming that the nonradiative processes are negligible at 14 K. Consequently, the IQE in a photoluminescence experiment is given by/estimated as $IQE \sim \frac{I_{PL}(RT)}{I_{PL}(14\ K)}$. Within the proposed classical model the evolution with temperature of the ion integrated intensity can be described according to $I(T)/I_0 = [1 + C\ exp\ (-E_a/k_B T)]^{-1}$, where T is the absolute temperature, I_0 the intensity at 14 K, C corresponds to the ratio of the electronic levels effective degeneracies and k_B the Boltzmann constant. Thus the determined IQE values and activation energies for the ion luminescence in the studied structures are indicated in Table 2. For the QWs the IQE value corresponds to the overall integrated intensity in the wavelength range of the $^3P_0 \rightarrow ^3F_2$ transition, which, as aforementioned corresponds to a region where an overlap of emitting centres occurs, hampering the calculation of the activation energies for the nonradiative processes of the individual centres. In the case of the NWs, and apart from the two values measured at the highest temperatures (where the integrated intensity calculation has a higher error), the Pr^{3+} emission intensity for the GaN NWs exhibits a high thermal stability up to 230 K. At this temperature still ~70% of the low temperature ion integrated intensity is observed for both fluences.

		GaN films	GaN NWs	AlN/GaN/AlN QWs	AlN/GaN(QDs)/AlN Superlattice
Transitions	Fluence (ions.cm^{-2})	Peak positions (±0.1 nm)			
$^3P_1 \rightarrow ^3H_5$	1×10^{13}	---	---	---	---
	1×10^{15}	---	---	526.6 529.4	526.6 527.2 529.7
$^3P_0 \rightarrow ^3H_5$	1×10^{13}	---	---	---	---
	1×10^{15}	---	---	532.6 537.3	532.6
$^3P_0 \rightarrow ^3F_2$	1×10^{13}	650.3 652.4 654.1 660.4	650.2 652.1 654.0 660.2	653.9 655.4 656.9 663.7	655.5 658.3 663.7
	1×10^{15}	650.3 652.4 654.1 660.4	650.2 652.1 654.0 660.2	655.6 663.7	654.6 655.6 658.7 663.7
$^3P_1 \rightarrow ^3F_3$	1×10^{13}	670.0 673.0 675.0 677.7	670.0 672.9	672.0	673.0
	1×10^{15}	669.9 672.9 675.0 677.7 680.1 682.5	670.0 672.9	673.1	673.2 678.0
$^3P_0 \rightarrow ^3F_3$	1×10^{13}	693.4	---	693.4	693.4
	1×10^{15}	693.6	---	693.4	693.4
$^1D_2 \rightarrow ^3H_5$	1×10^{13}	---	---	---	---
	1×10^{15}	695.1	---		696.9
$^3P_0 \rightarrow ^3F_4$	1×10^{13}	752.7 759.3 760.5	---	---	---
	1×10^{15}	752.7 757.4 759.3 760.5	---	755.5 757.0 765.7	757.1
$^1D_2 \rightarrow ^3H_6$	1×10^{13}	772.3 775.8 785.5	---	---	---
	1×10^{15}	772.2 775.8	---	780.1 788.9	781.9 788.9

	783.2 785.5 786.1 788.9

Table 1 – Assignments and peak position of the Pr^{3+} intra-shell lines for the studied samples.

	GaN films		GaN NWs		AlN/GaN/AlN QWs		AlN/GaN(QDs)/AlN Superlattice	
Fluence (ions.cm^{-2})	1×10^{13}	1×10^{15}	1×10^{13}	1×10^{15}	1×10^{13}	1×10^{15}	1×10^{13}	1×10^{15}
IQE (%)	14 %	43 %	43 %	42 %	13 %	25 %	39 %	15 %
E_a (meV)	11.6 ± 0.8	6.4 ± 0.4	5.3 ± 0.5	12.1 ± 2.1	---	---	43.1 ± 7.9	9.8 ± 1.6

Table 2 – IQE and E_a values for the $^3P_0 \rightarrow ^3F_2$ multiplet transitions of the Pr^{3+} ions in the studied samples.

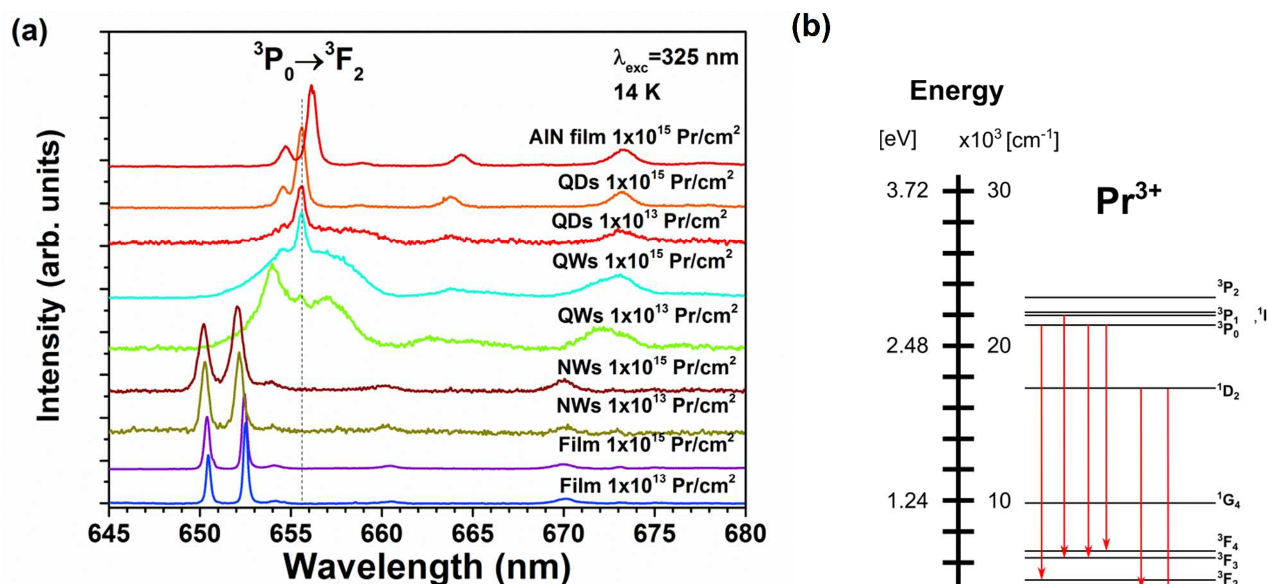

Figure 4 – (a) Comparison of the low temperature PL spectra of all the Pr^{3+} implanted samples. (b) Schematic energy band diagram of the Pr^{3+} free ion. The energy level were constructed based on reference [39].

A similar behaviour was found for the GaN layer implanted with the high fluence, corresponding to the sample displaying the most intense ion luminescence. In this case, ~80% of the ion integrated luminescence is still observed at ~230 K. The RT visual appearance of the intra-shell Pr^{3+} light emission in this layer is shown in Figure 6, together with the PLE spectrum which indicates that for the GaN layer the preferential excitation pathway for the Pr^{3+} luminescence is realized via above band gap excitation. The PL decay profile for the $^3P_0 \rightarrow ^3F_2$ transition measured at RT for the GaN layer is also shown in inset. The obtained results fit well to a single exponential decay with a lifetime of 21.9 μs as expected for a spin allowed transition, and this value is in good agreement with those previously reported [10]. The low luminescence intensity of the nanostructures at RT together with the low power Xe lamp used as excitation source for the PLE and lifetime measurements hampered the identification of the excitation lines/bands and the PL decay profile for the NWs, QWs and QDs. Furthermore, the high intensity of the intraionic luminescence enables, in this particular sample, the observation of additional intra-shell lines in the infrared spectral region, as shown in Figure 7. For the nanostructures (NWs, QWs and QDs) no emission lines were detected in this spectral region, even at low temperatures, due to the reduced visible/IR luminescence intensity.

Conclusions

Praseodymium implanted and annealed GaN samples were studied by photoluminescence. The optical activation of the ions was achieved in the all GaN structures (films, QWs, NWs and QDs) after thermal annealing. For all the samples the Pr^{3+} ion-related emission is dominated by the $^3P_0 \rightarrow ^3F_2$ transition. The film with high Pr content revealed a strong red emission even at RT, suggesting that high dopant concentration is necessary to reach intense emissions and the luminescence efficiency can be improved by annealing at high temperatures and high N_2-pressures, which minimizes the nonradiative processes.

 This journal is © The Royal Society of Chemistry 2014

For the NWs the peak position and spectral shape is in good agreement with the films, which proves the effective incorporation of the ion inside the GaN NWs. In the case of GaN QDs the intraionic emission appears to be mostly originated in the AlN layers used as spacers in the superlattice structure. In the QWs the sharp lines of the intraionic emission was found to be superimposed to a broad band likely due to the overlap of multiple Pr^{3+} centres caused by disorder-related effects after the implantation while the formation of intermixed AlGaN regions may give rise to additional centres with broad emission. The highest thermal stability of the emission intensity was obtained for the film implanted with the higher fluence and also for the low fluence-implanted NWs.

Acknowledgements

The authors acknowledge financial support from FCT: PTDC/CTM-NAN/2156/2012, PTDC/FIS-NAN/0973/2012, RECI/FIS-NAN/0183/2012 (FCOMP-01-0124-FEDER-027494) and Pest-C/CTM/LA0025/2013. J. Rodrigues, thanks to FCT for her PhD grant, SFRH/BD/76300/2011. K. Lorenz acknowledges funding by the program FCT Investigador.

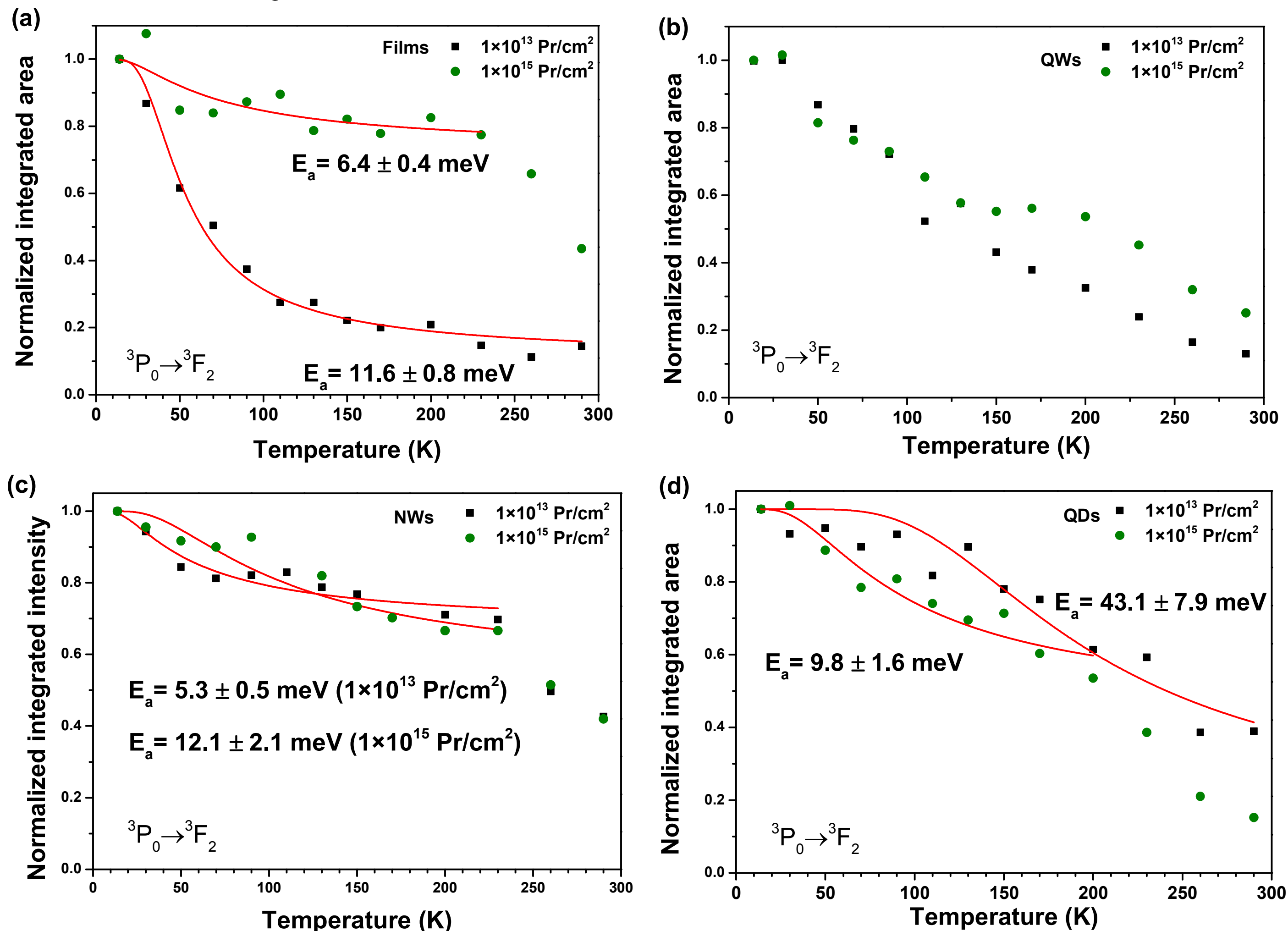

Figure 5 – Evolution of the integrated intensity for the GaN (a) films, (b) QWs (c) NWs and (d) QDs.

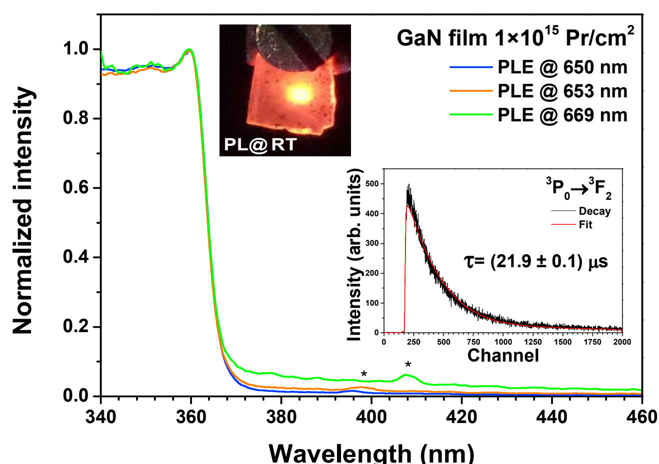

Figure 6 – RT PLE spectra of the GaN film implanted with higher fluence (the asterisks denote artefacts from the system). Insets: RT visual appearance of the intra-shell Pr^{3+} light emission in this layer; RT lifetime measurement for the $^3P_0 \rightarrow ^3F_2$ transition.

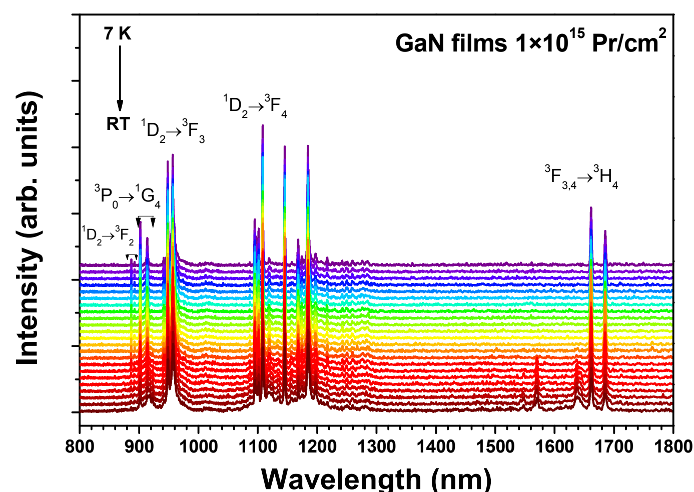

Figure 7 – Temperature dependent PL of the Pr^{3+} emission in the infrared region for the GaN film implanted with 1×10^{15} Pr/cm^2.

Notes

[a] Departamento de Física & I3N, Universidade de Aveiro, 3810-193 Portugal.*Email: joana.catarina@ua.pt
[b] IST, Instituto Superior Técnico, Campus Tecnológico e Nuclear, Universidade de Lisboa, EN10, 2695-066 Bobadela LRS, Portugal.
[c] IPFN, IST, Lisboa, Portugal.
[d] Univ. Grenoble Alpes, CEA/CNRS Group, "Nanophysique et Semiconducteurs", F-38000 Grenoble, France
[e] Institute of High Pressure Physics, Polish Academy of Sciences, 01-142 Warsaw, Poland

References

1. T. Suski, P. Perlin, H. Teisseyre, M. Leszczyński, I. Grzegory, J. Jun, M. Boćkowski, S. Porowski, and T. D. Moustakas, *Appl. Phys. Lett.*, 1995, **67**, 2188–2190.
2. P. Favennec and H. L'haridon, *Electron. Lett. Lett.*, 1989, **25**, 718–719.
3. M. R. Soares, J. Rodrigues, N. F. Santos, C. Nico, R. G. Carvalho, A. J. S. Fernandes, M. P. Graça, L. Rino, M. J. Soares, A. J. Neves, F. M. Costa, and T. Monteiro, in *SPIE OPTO*, eds. F. H. Teherani, D. C. Look, and D. J. Rogers, International Society for Optics and Photonics, 2013, p. 862607.
4. A. Wakahara, *Opt. Mater. (Amst).*, 2006, **28**, 731–737.
5. M. Peres, S. Magalhaes, N. Franco, M. Soares, A. Neves, E. Alves, K. Lorenz, and T. Monteiro, *Microelectronics J.*, 2009, **40**, 377–380.
6. K. P. O'Donnell, *Rare-Earth Doped III-Nitrides for Optoelectronic and Spintronic Applications*, Springer, 2009.
7. J. Rodrigues, S. M. C. Miranda, N. F. Santos, A. J. Neves, E. Alves, K. Lorenz, and T. Monteiro, *Mater. Chem. Phys.*, 2012, **134**, 716–720.
8. A. Nishikawa, T. Kawasaki, N. Furukawa, Y. Terai, and Y. Fujiwara, *Appl. Phys. express*, 2009, **2**, 1004.
9. A. Wakahara, Y. Nakanishi, T. Fujiwara, A. Yoshida, T. Ohshima, and T. Kamiya, *Phys. status solidi*, 2005, **202**, 863–867.
10. H. J. Lozykowski, W. M. Jadwisienczak, and I. Brown, *J. Appl. Phys.*, 2000, **88**, 210.
11. R. Birkhahn, M. Garter, and A. J. Steckl, *Appl. Phys. Lett.*, 1999, **74**, 2161.
12. J. M. Zavada, R. A. Mair, C. J. Ellis, J. Y. Lin, H. X. Jiang, R. G. Wilson, P. A. Grudowski, and R. D. Dupuis, *Appl. Phys. Lett.*, 1999, **75**, 790.
13. E. Alves, K. Lorenz, R. Vianden, C. Boemare, M. J. Soares, and T. Monteiro, *Mod. Phys. Lett. B*, 2001, **15**, 1281–1287.
14. E. Schultheiss, A. Scharmann, and D. Schwabe, *Phys. status solidi*, 1987, **140**, 173–189.
15. L. Esterowitz, F. Bartoli, R. Allen, D. Wortman, C. Morrison, and R. Leavitt, *Phys. Rev. B*, 1979, **19**, 6442–6455.
16. S. Li and A. Waag, *J. Appl. Phys.*, 2012, **111**, 071101–071101–23.
17. J. Rodrigues, S. M. C. Miranda, A. J. S. Fernandes, E. Nogales, L. C. Alves, E. Alves, G. Tourbot, T. Auzelle, B. Daudin, B. Méndez, T. Trindade, K. Lorenz, F. M. Costa, and T. Monteiro, *Phys. status solidi*, 2013, **10**, 667–672.
18. J. Brault, T. Huault, F. Natali, B. Damilano, D. Lefebvre, M. Leroux, M. Korytov, and J. Massies, *J. Appl. Phys.*, 2009, **105**, 033519.
19. M. Peres, S. Magalhães, V. Fellmann, B. Daudin, A. Neves, E. Alves, K. Lorenz, and T. Monteiro, *Nanoscale Res. Lett.*, 2011, **6**, 378.

This journal is © The Royal Society of Chemistry 2014

20. B. Damilano, N. Grandjean, F. Semond, J. Massies, and M. Leroux, *Appl. Phys. Lett.*, 1999, **75**, 962.

21. J. M. Gérard, O. Cabrol, and B. Sermage, *Appl. Phys. Lett.*, 1996, **68**, 3123.

22. S. Magalhães, M. Peres, V. Fellmann, B. Daudin, A. J. Neves, E. Alves, T. Monteiro, and K. Lorenz, *J. Appl. Phys.*, 2010, **108**, 084306.

23. A. Redondo-Cubero, K. Lorenz, E. Wendler, D. Carvalho, T. Ben, F. M. Morales, R. García, V. Fellmann, and B. Daudin, *Nanotechnology*, 2013, **24**, 505717.

24. I. S. Roqan, K. P. O'Donnell, R. W. Martin, P. R. Edwards, S. F. Song, A. Vantomme, K. Lorenz, E. Alves, and M. Bockowski, *Phys. Rev. B*, 2010, **81**, 085209.

25. K. Lorenz, S. M. C. Miranda, E. Alves, I. S. Roqan, K. P. O'Donnell, and M. Bokowski, in *SPIE OPTO*, International Society for Optics and Photonics, 2012, p. 82620C–82620C–6.

26. O. Landré, C. Bougerol, H. Renevier, and B. Daudin, *Nanotechnology*, 2009, **20**, 415602.

27. K. Lorenz, E. Nogales, S. M. C. Miranda, N. Franco, B. Méndez, E. Alves, G. Tourbot, and B. Daudin, *Acta Mater.*, 2013, **61**, 3278–3284.

28. J. Bartels, K. Freitag, J. G. Marques, J. C. Soares, and R. Vianden, *Hyperfine Interact.*, 1999, **120-121**, 397–402.

29. B. Daudin, F. Widmann, G. Feuillet, Y. Samson, M. Arlery, and J. Rouvière, *Phys. Rev. B*, 1997, **56**, R7069–R7072.

30. M. Arlery, J. L. Rouvière, F. Widmann, B. Daudin, G. Feuillet, and H. Mariette, *Appl. Phys. Lett.*, 1999, **74**, 3287.

31. M. Peres, S. Magalhães, J. Rodrigues, M. J. Soares, V. Fellmann, A. J. Neves, E. Alves, B. Daudin, K. Lorenz, and T. Monteiro, *Opt. Mater. (Amst).*, 2011, **33**, 1045–1049.

32. D. Chen, J. Wang, D. Xu, and Y. Zhang, *Vacuum*, 2009, **83**, 865–868.

33. B. Berzina, L. Trinkler, J. Grabis, and I. Steins, *Phys. status solidi*, 2007, **4**, 959–962.

34. M. A. Reshchikov and H. Morkoç, *J. Appl. Phys.*, 2005, **97**, 061301–061301–95.

35. R. Seitz, C. Gaspar, T. Monteiro, E. Pereira, M. Leroux, B. Beaumont, and P. Gibart, *MRS Int. J. Nitride Semicond. Res.*, 1997, **2**.

36. J. Rodrigues, S. M. C. Miranda, M. Peres, E. Nogales, L. C. Alves, E. Alves, G. Tourbot, B. Daudin, B. Méndez, K. Lorenz, and T. Monteiro, *Nucl. Instruments Methods Phys. Res. Sect. B Beam Interact. with Mater. Atoms*, 2013, **306**, 201–206.

37. H. J. Lozykowski, W. M. Jadwisienczak, A. Bensaoula, and O. Monteiro, *Microelectronics J.*, 2005, **36**, 453–455.

38. C. Leclere, V. Fellmann, C. Bougerol, D. Cooper, B. Gayral, M. G. Proietti, H. Renevier, and B. Daudin, *J. Appl. Phys.*, 2013, **113**, 034311.

39. W. T. Carnall, *J. Chem. Phys.*, 1968, **49**, 4424.

This journal is © The Royal Society of Chemistry 2014